Electrochemistry Communications 177 (2025) 107960

Contents lists available at ScienceDirect

Electrochemistry Communications

journal homepage: www.elsevier.com/locate/elecom

Short communication

Unraveling ionic transport in polymer-ceramic electrolytes: Insights into superionic interphases

F. Gerbig [a],*,[1], N. Röttgen [b],*,[1], M. Holzapfel [b], G. Dück [c], M. Finsterbusch [c], H. Nirschl [a]

[a] Institute of Mechanical Process Engineering and Mechanics, Karlsruhe Institute of Technology (KIT), Straße am Forum 8, Karlsruhe, 76131, Germany
[b] Fraunhofer Institute for Chemical Technology (ICT), Joseph-von-Fraunhofer-Straße 7, Pfinztal, 76327, Germany
[c] Institute of Energy Materials and Devices (IMD-2), Forschungszentrum Jülich GmbH, Wilhelm-Johnen-Straße, Jülich, 52425, Germany

ARTICLE INFO

Keywords:
Solid electrolytes
NaSICON
PEO
Microstructure
Modeling and simulation

ABSTRACT

This study investigates the transport phenomena in composite solid electrolytes (CSEs) based on polyethylene oxide (PEO) and ceramic fillers for sodium-ion batteries. Numerical microstructure simulations, paired with experimental conductivity measurements, were conducted to explore the mechanisms of ionic transport in these materials. Incorporating $Na_{3.4}Zr_2Si_{2.4}P_{0.6}O_{12}$ into a PEO matrix did not significantly enhance ionic conductivity compared to the pure polymer. However, a CSE containing $Na_3Zr_2Si_{2.3}P_{0.7}O_{11.85}$ showed notable improvements in conductivity. Despite these enhancements, the measured conductivities remained lower than predicted by models assuming full ionic transport through both the polymer and ceramic phases, suggesting that the assumption of complete charge transport through the ceramic filler is overly optimistic. The data suggests that amorphization in the PEO matrix induced by ceramic fillers is not the main driver for enhanced ionic conductivity of the CSE, as improvements were observed at both room temperature and above the glass transition temperature of PEO. A more plausible explanation for the observed conductivity enhancement lies in the presence of a superionic interphase at the polymer–ceramic interface. Simulations suggest that this interphase, with submicrometer thickness and ionic conductivity higher than those of the bulk PEO, plays a significant role in facilitating ion transport.

1. Introduction

Rechargeable batteries are essential to the expansion of electric vehicles and battery-based grid storage systems, both of which are critical for mitigating climate change [1]. While the anode and cathode materials typically receive the most attention in battery research, the electrolyte plays an equally vital role in determining the performance and functionality of the battery cell. The electrolyte's importance extends beyond its primary function as an ionic conductor between electrodes; it also significantly influences the battery's efficiency, safety, and lifespan [2].

Solid electrolytes have attracted growing interest due to their ability to eliminate issues associated with liquid electrolytes, such as leakage and volatilization. Additionally, solid electrolytes promise improved long-term stability and enhanced safety. Their inherent mechanical strength also offers the potential to enable the use of metal anodes in lithium-ion and sodium-ion batteries, which could further improve battery performance [3–5]. However, single-phase solid electrolytes often struggle to meet the comprehensive requirements for practical alkali metal ion batteries. These requirements include thermal and mechanical stability, high ionic conductivity, low interfacial resistance, and excellent electrochemical stability [6]. Achieving all of these properties simultaneously in a single material remains a challenge due to the inherent limitations of each solid electrolyte.

Composite solid electrolytes (CSEs), especially those integrating polymer electrolytes with inorganic solid electrolytes and known as composite polymer electrolytes (CPE), have emerged as viable alternatives. By leveraging the complementary properties of the individual components, CSEs can potentially address the trade-offs seen in single-phase electrolytes. However, the detailed mechanisms governing ion transport in CPEs remain unclear [7].

One proposed mechanism for this enhancement is the modification of defect thermodynamics near the polymer-crystal interface [8].

In some materials, the interface between the polymer and filler can form a new phase known as the *interphase*, which acts as a fast-ion conducting channel within the sub-micrometer range as found by Liu et al. between LiBFSIE and LLZO [9] (see schematic in Fig. 1).

* Corresponding authors.
E-mail addresses: felix.gerbig@kit.edu (F. Gerbig), niklas.roettgen@ict.fraunhofer.de (N. Röttgen).
[1] Authors contributed equally.

https://doi.org/10.1016/j.elecom.2025.107960
Received 6 April 2025; Received in revised form 6 May 2025; Accepted 10 May 2025
Available online 28 May 2025

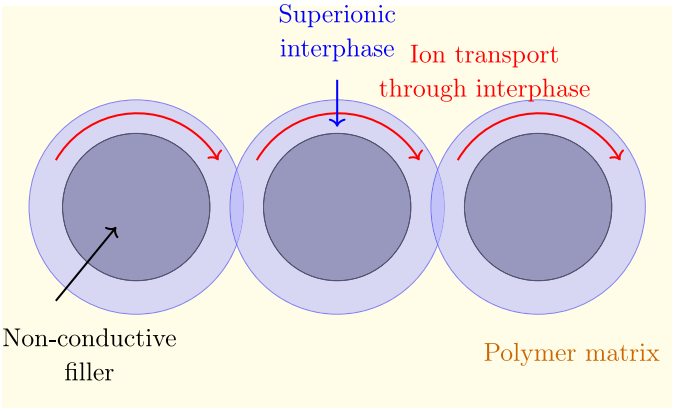

Fig. 1. Schematic of ion transport in composite solid electrolytes. The ceramic fillers (gray) are surrounded by superionic interphases (blue). Enhanced ion transport (red arrows) occurs through these interphase regions, following curved paths along the shell boundaries. The surrounding polymer matrix is shown in light yellow. The relative dimensions are exaggerated for clarity, especially the interphase thickness.

Rather than differentiating between fillers that enhance transport at the interface and those that form interphases Xu et al. argue that the observed differences in conduction mechanisms are related to the radial extent of the fast-ion conducting zone around the filler particles [10, 11].

Another perspective suggests that fillers induce structural changes in the polymer host, creating a more favorable environment for ion conduction. This is attributed to the stabilization of highly-conductive amorphous phases at room temperature, which usually form at temperatures above 60 °C for PEO-based electrolytes [12,13].

This lack of understanding of the precise ion transport mechanisms in CPEs hinders the accurate prediction of conductivity and slows the progress of research in this area. To better understand the charge transport phenomena in CPEs, numerical simulations of their microstructures were conducted and compared with experimental conductivity measurements of both the CSE and its constituent single-phase electrolytes in this work. The study was carried out using the example of materials for sodium-ion batteries, one of the most promising future battery technologies.

2. Materials and methods

2.1. NaSICON synthesis

NaSICON powders were synthesized via solution-assisted solid-state-reaction (SA-SSR) following [14–16]. For slightly sub-stoichiometric NaSICON ($Na_3Zr_2Si_{2.3}P_{0.7}O_{11.85}$), stoichiometric solutions of Na_2SiO_3 (> 98%, Sigma-Aldrich) and $NH_4H_2PO_4$ (98 %, Alfa-Aesar) in deionized water were mixed. A solution of $ZrO(NO_3)_2$ was then added under stirring, and the remaining Si was incorporated via $Si(OC_2H_5)_4$ (TEOS) (99 %, Sigma-Aldrich), forming a sol. The pH was adjusted to 3 with HNO_3. After 3 h of stirring, the mixture was heated to 80 °C to remove water, followed by drying at 110 °C overnight. The dried material was crushed and ball-milled at 300 rpm for 2 h to 3 h using zirconia media. The powder was calcined at 750 °C for 4 h (100 °C h^{-1}), milled again, and sintered at 1150 °C for 5 h (200 °C h^{-1}). For NaSICON with higher sodium content ($Na_{3.4}Zr_2Si_{2.4}P_{0.6}O_{12}$), NaNO3 (Merck) was used, with calcination at 800 °C and sintering at 1260 °C.

Powder diffraction data were collected at ambient conditions using a Bruker D8 DaVinci diffractometer with Cu-Kα radiation and a Lynx-Eye PSD detector. Data were measured in the 5° to 50° 2θ range. Phase assignment was based on the PDF-2 powder diffraction database (Version 1999). Entry numbers in Fig. 2 correspond to phases assigned using the best figure of merit for lattice metric matching.

These assignments are structural matches rather than exact compositional matches, as the database entries may represent materials with significant solid solution ranges. Figs. 2(a) and 2(b) display the X-ray diffraction patterns, indicating a nearly pure NaSICON phase in $Na_3Zr_2Si_{2.3}P_{0.7}O_{11.85}$ and the presence of less than 10 % secondary phases in $Na_{3.4}Zr_2Si_{2.4}P_{0.6}O_{12}$, respectively.

2.2. Preparation of SPE and CSE membranes

SPE and CSE membranes were fabricated by solution casting. NaTFSI (99.5 %, Solvionic) and the crosslinking initiator (Irgacure819®, BASF) were dissolved in acetonitrile (anhydrous, Sigma-Aldrich) under stirring, followed by stepwise polymer (CP-A1H, Alroko GmbH) addition to form a slurry. The solvent-to-polymer ratio was 2 mL g^{-1} to 2.5 mL g^{-1}, and the polymer-to-NaTFSI molar ratio was 20:1, with 0.5 wt % crosslinking initiator. After stirring for 4 h to 5 h, the slurry was cast onto PTFE sheets using a doctor blade (wet-film thickness: 500 µm).

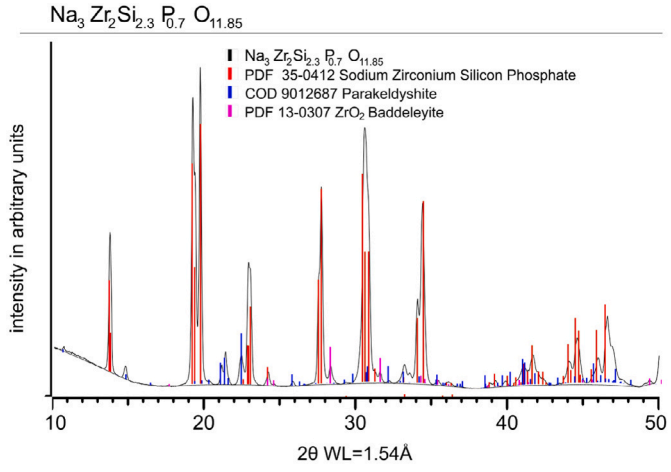

(a) XRD of $Na_3Zr_2Si_{2.3}P_{0.7}O_{11.85}$

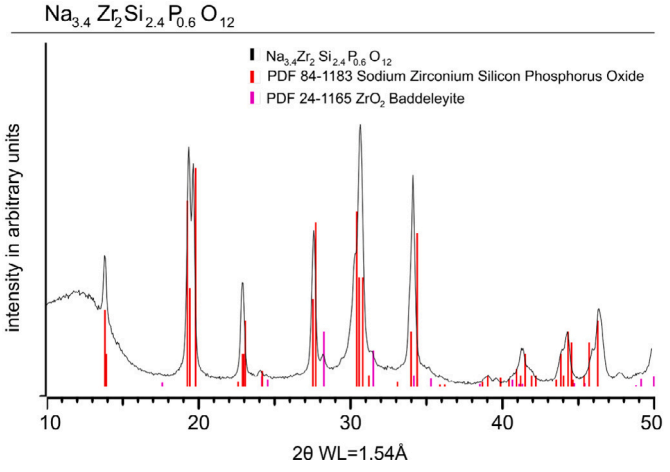

(b) XRD of $Na_{3.4}Zr_2Si_{2.4}P_{0.6}O_{12}$

Fig. 2. X-ray diffraction patterns of used NaSICON materials.

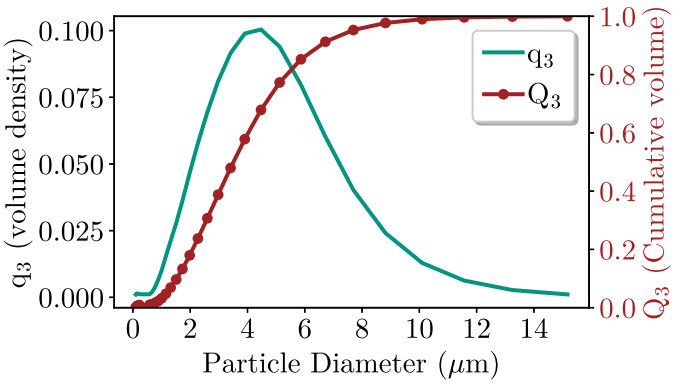

Fig. 3. Measured particle size distribution of NaSICON particles used in the microstructure simulations, showing both the density distribution and the cumulative sum distribution of particle sizes, based on volume.

The solvent evaporated at room temperature, and the film was UV-irradiated for 10 min for crosslinking, followed by drying at 80 °C under vacuum. For CSE membranes, NaSICON powder (50 wt %) was added to the SPE components and dispersed using a high-shear mixer (Thinky) and ultrasonic bath (10 min). All preparation steps were conducted in an argon-filled glovebox or under sealed argon containers.

2.3. Conductivity measurements

Temperature-dependent conductivity was measured on electrolyte membranes (21 mm diameter) placed between stainless steel electrodes in a PAT-cell® (EL-CELL GmbH). Samples were conditioned at 80 °C for 7.5 h to improve electrode contact, and impedance measurements were performed while lowering the temperature in 10 °C steps (down to 25 °C). Impedance was measured with a potentiostat (VSP3e, Biologic) in the 700 kHz to 10 Hz range, using 13 points per decade. Ionic transport resistances were extracted using RelaxIS 3 (rhd instruments GmbH) and used to calculate conductivity (κ) via:

$$\kappa = \frac{L}{AR} \tag{1}$$

where L is membrane thickness, R is ionic resistance, and A is the contact area. Membrane thickness was measured with a micrometer gauge (90 μm to 130 μm), with variations below 10 μm.

2.4. Numerical method

CSE microstructures were generated using the Discrete Element Method (DEM) in LIGGGHTS, adapted from Chauhan et al. [17]. This method simulated random assemblies of 1000 dense, spherical NaSICON particles in a polymer matrix. The computational domain was reduced to final dimensions of 135 μm×45 μm×45 μm to mimic solvent casting, focusing on the geometric arrangement rather than particle interactions. The mesh was generated in OpenFOAM® with a structured hexagonal grid and minimal errors, solved using a second-order finite-volume method and geometric-algebraic multigrid solver.

The numerical solver used in this study is adapted from a previously developed all-solid-state sodium-ion battery model by the authors, as detailed in [18]. It is employed to solve the charge conservation equation:

$$0 = \nabla\kappa\nabla\Phi_{el} \tag{2}$$

Boundary conditions were applied by fixing the potential at both ends of the domain ($\Phi_{el,x=L}$ and $\Phi_{el,x=0}$), typically assigning 1 V. Effective ionic conductivity (κ_{eff}) was calculated as:

$$\kappa_{eff} = \frac{L\left|i_{el,x=L}\right|}{A\left(\Phi_{el,x=L} - \Phi_{el,x=0}\right)} \tag{3}$$

Table 1
Measured conductivity of single phase solid electrolytes and composite solid electrolytes employed in this study.

	κ(25 °C) (S m^{-1})	κ(80 °C) (S m^{-1})
PEO	5.5×10^{-4}	8.9×10^{-2}
$Na_3Zr_2Si_{2.3}P_{0.7}O_{11.85}$	1.7×10^{-1}	7.9×10^{-1}
$Na_{3.4}Zr_2Si_{2.4}P_{0.6}O_{12}$	3.4×10^{-1}	1.7
PEO (50 wt %)/$Na_3Zr_2Si_{2.3}P_{0.7}O_{11.85}$ (50 wt %)	1.13×10^{-3}	1.4×10^{-1}
PEO (50 wt %)/$Na_{3.4}Zr_2Si_{2.4}P_{0.6}O_{12}$ (50 wt %)	6.4×10^{-4}	5.4×10^{-2}

The particle size distribution, shown in Fig. 3, was monomodal with a median size (d_{50}) of 3.5 μm. Particles smaller than 1 μm were excluded from the analysis to maintain mesh resolution, with their contribution to the total surface area below 0.25 %.

3. Results and discussion

The primary objective of this work is to compare experimentally measured ionic conductivities with predictions generated by the numerical solver used throughout the study. By simulating the effective conductivity, we aim to shed light on the role of polymer–ceramic interactions in enhancing ionic transport. To isolate the effects of the CSE structure itself, all experiments and simulations were conducted using a pure electrolyte material, with no active electrode materials involved.

The experimentally measured conductivities of the SPEs are listed in the first three rows of Table 1. In this context, conductivity measurements for $Na_{3.4}Zr_2Si_{2.4}P_{0.6}O_{12}$ showed no significant enhancement over the conductivity of PEO alone: At 80 °C, the conductivity of the CSE decreases to 5.4×10^{-2} S m^{-1}, while for PEO, it is 8.9×10^{-2} S m^{-1}. This suggests that the NaSICON sample does not participate in the Na^+ transport, reducing the effective conductivity due to elongated ion transport paths and increased porosity. At 25 °C, below the melting temperature of the quasicrystalline phase, the CSE conductivity (6.4×10^{-4} S m^{-1}) becomes similar to that of the SPE (5.5×10^{-4} S m^{-1}). This may be attributed to a level of PEO amorphization that mitigates the adverse effects of the filler particles in this scenario.

In contrast, the $Na_3Zr_2Si_{2.3}P_{0.7}O_{11.85}$ containing CPE shows drastically increased conductivity compared to pure PEO. Fig. 4 shows a comparison between the experimentally measured and simulated conductivities for the polymer–ceramic CSE at 25 °C. The experimental conductivity of the composite (1.13×10^{-3} S m^{-1}) lies between the conductivities of pure PEO and NaSICON (dotted lines). The simulated conductivity, assuming full ionic transport through both phases, is significantly higher (7.78×10^{-3} S m^{-1}), indicating that complete ionic transport through all phases may be an unrealistic assumption.

To explore alternative explanations, we tested a hypothesis in which ionic transport occurs primarily within a superionic interphase surrounding the ceramic filler particles rather than through the ceramic itself. In these simulations, filler particles were treated as non-conductive, while the adjacent PEO matrix was assigned enhanced conductivity. Interphase thickness and conductivity were varied systematically to assess whether certain combinations could reproduce the experimentally observed CSE conductivity. The results, shown as solid lines with markers in Fig. 4, indicate that interphase-dominated transport can account for the measured conductivity.

The total conductivity displays a linear relationship with the interphase conductivity in a double logarithmic graph. As a result, the point at which the regression line intersects the measured conductivity curve corresponds to a specific pair of interphase thickness and conductivity. For instance, a 125 nm interphase with a conductivity of 5.5×10^{-2} S m^{-1}, a 250 nm interphase with a conductivity of 2.15×10^{-2} S m^{-1}, or a 500 nm interphase with a conductivity of 8.6×10^{-3} S m^{-1} are all potential configurations that match the experimental data. These

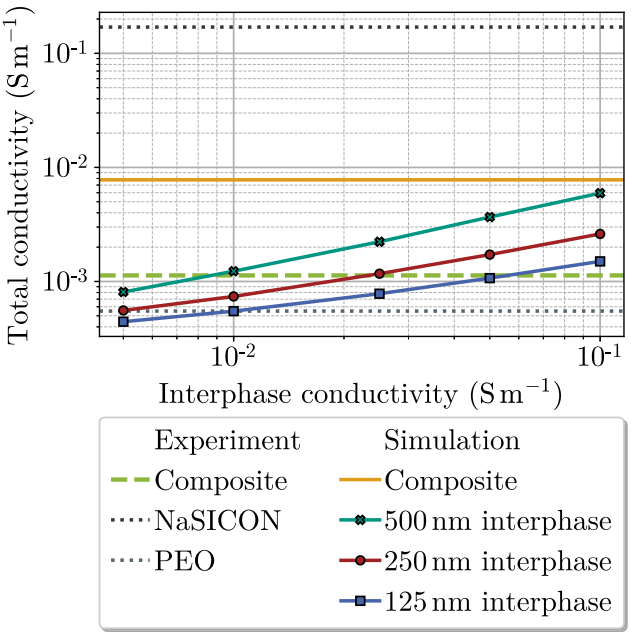

Fig. 4. Comparison of total ionic conductivity as a function of interphase conductivity between experimental data and simulations for NaSICON-PEO composite electrolytes. Experimental data for NaSICON (gray dotted line), PEO (black dotted line), and the CSE (green dashed line) are shown alongside simulation results for full ion transport (yellow solid line) and interphase thicknesses ranging from 500 nm to 125 nm (solid lines with markers) at 25 °C.

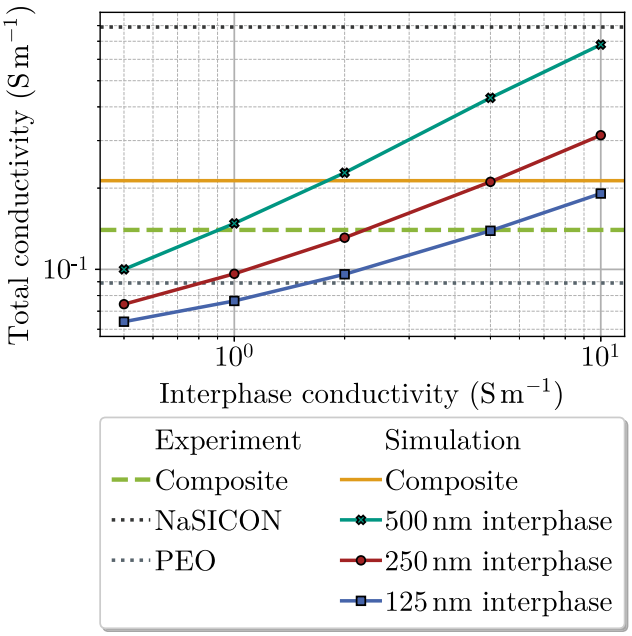

Fig. 5. Comparison of total ionic conductivity as a function of interphase conductivity between experimental data and simulations for NaSICON-PEO composite electrolytes. Experimental data for NaSICON (gray dotted line), PEO (black dotted line), and the CSE (green dashed line) are shown alongside simulation results for full ion transport (yellow solid line) and interphase thicknesses ranging from 500 nm to 125 nm (solid lines with markers) at 80 °C.

results suggest that ionic transport in this sample is likely confined to a superionic interphase, rather than occurring throughout the ceramic filler particles.

To investigate the hypothesis that fillers enhance conductivity by inducing amorphous regions in the PEO matrix, which stabilize at ambient temperature, a similar experiment was conducted at 80 °C—a temperature above PEO's glass transition point, where the polymer is predominantly in its amorphous phase. The results are illustrated in Fig. 5. As anticipated, the conductivities of both single-phase electrolytes grow with increasing temperature; notably, the PEO conductivity surges by over two orders of magnitude. Significantly, the CSE conductivity is more than twice as high as the conductivity of pure PEO. This challenges the theory that attributes the conductivity enhancement mainly to fillers inducing structural changes in the PEO bulk because PEO is already in an amorphous state at 80 °C.

However, the simulation assuming full charge transport in the NaSICON still overestimates the effective conductivity, albeit to a lesser extent than at 25 °C. Consistent with the observations at 25 °C, disregarding ionic transport within the ceramic phase and instead incorporating superionic interphases aligns well with the experimental results at 80 °C. The thicknesses and conductivities of the interphases, such as 125 nm with a conductivity of 4.84 S m^{-1}, 250 nm with 2.06 S m^{-1}, or 500 nm with 0.88 S m^{-1}, can account for the measured values.

Interestingly, the interphase conductivity is approximately halved relative to the PEO conductivity at 80 °C compared to 25 °C. This could be due to the relatively low PEO conductivity at ambient temperature or may reflect an upper limit for the conductivity of the interphase itself. These findings highlight the need for further experimental work to better understand the temperature dependence of ionic transport in polymer–ceramic CSE.

4. Conclusion

The analysis of transport phenomena in PEO-based polymer–ceramic electrolytes offers key insights into the role of active fillers in facilitating ionic transport. Notably, incorporating $Na_{3.4}Zr_2Si_{2.4}P_{0.6}O_{12}$ into a PEO matrix did not lead to a substantial conductivity enhancement relative to the single-phase electrolyte (SPE). In contrast, a CSE containing $Na_3Zr_2Si_{2.3}P_{0.7}O_{11.85}$ exhibited improved conductivity; however, measured values remained below those predicted by models assuming ideal ion transport through both the polymer and ceramic phases. These results suggest that the assumption of full charge transport through the ceramic filler may be overly simplistic. Moreover, attributing the conductivity enhancement solely to polymer amorphization near the ceramic particles appears inadequate, as the effect persists even above the PEO glass transition temperature.

A more consistent explanation arises from the formation of a superionic interphase at the polymer–ceramic interface. Simulations that attribute the observed conductivity enhancement solely to this interphase yielded realistic values for interphase thickness in the submicron range and interphase conductivities. For instance, an interphase of 125 nm with a conductivity of 5.5×10^{-2} S m^{-1} at 25 °C aligns well with the experimental data. Interestingly, XRD data indicate the presence of minor secondary phases in the substoichiometric NaSICON, which could play a role in the enhanced conductivity. Further studies are encouraged to explore this hypothesis.

CRediT authorship contribution statement

F. Gerbig: Writing – review & editing, Writing – original draft, Visualization, Validation, Software, Methodology, Investigation, Formal analysis, Conceptualization. **N. Röttgen:** Writing – review & editing, Validation, Methodology, Investigation, Formal analysis, Data curation. **M. Holzapfel:** Resources, Project administration. **G. Dück:** Investigation. **M. Finsterbusch:** Supervision, Resources, Project administration. **H. Nirschl:** Resources, Project administration.

Declaration of Generative AI and AI-assisted technologies in the writing process

During the preparation of this work the authors used OpenAI's ChatGPT (based on the GPT-4 architecture) in order to assist in the

grammar and language review of this manuscript. After using this tool, the authors reviewed and edited the content as needed and take full responsibility for the content of the published article.

Declaration of competing interest

The authors declare that they have no known competing financial interests or personal relationships that could have appeared to influence the work reported in this paper.

Acknowledgments

The authors acknowledge funding and support from the German Federal Ministry of Education and Research (Bundesministerium für Bildung und Forschung) in the joint project Hyperium under project number 03XP0403A-D. Additionally, the authors want to thank Dr. Peter Schultz for the XRD measurements and the insightful discussion of the results. The responsibility for the content is with the authors. Additionally, this research received support from the state of Baden-Württemberg through bwHPC.

Data availability

Data will be made available on request.

References

[1] T.M. Gür, Energy & Environ. Sci. 11 (10) (2018) 2696–2767.
[2] G.G. Eshetu, et al., Adv. Energy Mater. 10 (20) (2020) 2000093.
[3] C. Bao, et al., Adv. Funct. Mater. 30 (52) (2020) 2004891.
[4] S. Vasudevan, S. Dwivedi, P. Balaya, Int. J. Appl. Ceram. Technol. 20 (2) (2023) 563–584.
[5] D.A. Edelman, T.G. Brandt, E. Temeche, R.M. Laine, Mater. Today Commun. 32 (2022) 104009.
[6] S. Kumar, R. Raghupathy, M. Vittadello, Batter. 10 (3) (2024) 73.
[7] Z. Zou, et al., Chem. Rev. 120 (9) (2020) 4169–4221.
[8] R.C. Agrawal, R.K. Gupta, J. Mater. Sci. 34 (6) (1999) 1131–1162.
[9] K. Liu, et al., ACS Energy Lett. 6 (4) (2021) 1315–1323.
[10] X. Xu, et al., ChemSusChem 16 (8) (2023) e202202152.
[11] P.M. Veelken, et al., Nanomater. (Basel, Switzerland) 12 (4) (2022) 654.
[12] D. Lei, et al., Nat. Commun. 10 (1) (2019) 4244.
[13] A. Karmakar, A. Ghosh, J. Nanoparticle Res. 13 (7) (2011) 2989–2996.
[14] J.P. Gross, et al., J. Mater. Sci. 58 (1) (2023) 144–157.
[15] M. Holzapfel, D. Wilde, C. Hupbauer, K. Ahlbrecht, T. Berger, Electrochim. Acta 237 (2017) 12–21.
[16] S. Naqash, Q. Ma, F. Tietz, O. Guillon, Solid State Ion. 302 (2017) 83–91.
[17] A. Chauhan, E. Asylbekov, S. Kespe, H. Nirschl, Electrochem. Sci. Adv. 3 (1) (2023) e2100151.
[18] F. Gerbig, A. Chauhan, S. Gietl, H. Nirschl, J. Electrochem. Soc. 171 (9) (2024) 090515.